# Adaptive Constrained On-board Guidance Technology for Powered Glide Vehicle

*Huang Rong*[1,2*], *Wei Changzhu*[1], *Liu Yanbin*[3], *Lu Yuping*[3]

1. School of Astronautics, Harbin Institute of Technology, Harbin 150001, P. R. China;
2. Beijing Institute of Control and Electronic Technology, Beijing 100038, P. R. China;
3. College of Astronautics, Nanjing University of Aeronautics and Astronautics, Nanjing 210016, P. R. China

(Received 14 February 2016; revised 16 March 2016; accepted 25 April 2016)

**Abstract**: To make full use of expanded maneuverability and increased range, adaptive constrained on-board guidance technology is the key capability for a glide vehicle with a double-pulse rocket engine, especially under the requirements of desired target changing and on-line reconfigurable control and guidance. Based on the rapid footprint analysis, whether the new target is within the current footprint area is firstly judged. If not, the rocket engine ignites by the logic obtained from the analysis of optimal flight range by the method of hp-adaptive Gauss pseudospectral method (hp-GPM). Then, an on-board trajectory generation method based on powered quasi-equilibrium glide condition (QEGC) and linear quadratic regulator (LQR) method is used to guide the vehicle to the new target. The effectiveness of the guidance method consisted of powered on-board trajectory generation, LQR trajectory tracking, footprint calculation, and ignition time determination is indicated by some simulation examples.

**Key words**: adaptive constrained on-board guidance; double-pulse rocket engine; hp-adaptive Gauss pseudospectral method; powered quasi-equilibrium glide condition; linear quadratic regulator (LQR) trajectory tracking

**CLC number**: V249.1 **Document code**: A **Article ID**: 1005-1120(2017)02-0125-09

## 0 Introduction

Along with the development of practical designs for a pulse solid rocket engine, the application and study of powered glide vehicles are promoted. A multi-pulse rocket engine is able to effectively increase the flight range and terminal velocity of the glide vehicle[1,2], which means it can reach much wider targets. In order to make full use of the mobility and long range of powered glide vehicles, a more deep research on adaptive constrained on-board guidance technology is necessary, especially for the situation that target is changed during flight.

With the advance in on-board computational capability, the predictor-corrector guidance algorithms have received increasing attention[3,4]. The main advantage over more traditional entry guidance approaches is the elimination of the need for a prestored reference trajectory that the current state can differ significantly from, either due to dispersions or off-nominal conditions. However, a prevalent shortcoming in the existing predictor-corrector algorithms has been the lack of a effective means to enforce inequality trajectory constraints. To directly enforce inequality trajectory constraints by parameterizing the trajectory control, the number of the unknown parameters will inevitably have to be increased, which will have significant adverse effects on the speed and robustness of the algorithm, rendering the approach impractical for on-board applications[5-7].

* Corresponding author, E-mail address: I_amhuangrong@163.com.

**How to cite this article**: Huang Rong, Wei Changzhu, Liu Yanbin, et al. Adaptive constrained on-board guidance technology for powered glide vehicle[J]. Trans. Nanjing Univ. Aero. Astro., 2017,34(2):125-133.
http://dx.doi.org/10.16356/j.1005-1120.2017.02.125

This paper investigates a fully constrained predictor-corrector guidance algorithm for powered glide vehicles subject to any feasible inequality trajectory constraints in the velocity-altitude space without increasing complexity and reducing the robustness of the guidance algorithm. The powered quasi-equilibrium glide condition (QEGC) yielding a velocity-dependent upper bound on the magnitude of the bank angle is compensated with small corrections to improve its accuracy at higher altitudes and allow better shaping of the trajectory for heating constraint enforcement, the complexity of which is significantly less and the structure more streamlined than the algorithm in Refs. [8, 9]. Furthermore, a powered on-board trajectory generation method is developed. Afterwards, the linear quadratic regulator (LQR) method is used to track the on-board generation reference trajectory.

Compared with the unpowered glide vehicles, powered glide vehicles can reach the new targets not in current footprint by multi-pulse rocket engine ignition. Therefore, footprint and ignition time analysis is necessary for the guidance of powered glide vehicles.

Footprint is the set of all the reachable landing spots of vehicle with given initial, path, and terminal constraints, whose boundary points are the end points of optimal trajectories. The challenge in developing an algorithm to calculate the landing footprint is to find a method that simplifies the calculations, yet generates a sufficiently close approximation to the actual landing footprint[10]. There are four typical methods by which the footprint has been successfully obtained[11]. Inspired by the acceleration-energy profile[12], a footprint analysis method based on velocity-bank angle profile is proposed.

The complete solution to the optimal pulse engine problem involves simultaneous optimization of the engine parameters, ignition time, and trajectory shaping. Two broad approaches[13-15] are available for solution of this problem: Parameter optimization of complete problem and analytical solution of reduced-order model. The engine parameters of the vehicle studied here are fixed, which means only ignition time and trajectory shaping are optimization variables. And an hp-adaptive Gauss pseudospectral method[16-18], which can effectively handle problems with discontinuous dynamics, is employed to give an optimal analysis of variation between range and ignition time of the pulse engine.

Accordingly, the flow of adaptive constrained on-board guidance for powered glide vehicles is given in Fig. 1. When a target-changed order is received, whether the new target is within the footprint area is firstly judged by footprint analysis method based on velocity-bank angle profile. If it is not, the rocket engine ignites by the logic obtained from the analysis of optimal flight range. Then, an on-board trajectory generation method based on the powered QEGC and the LQR method is used to guide the vehicle to the new target. Numerical results are presented to evaluate the efficiency and accuracy of the approach.

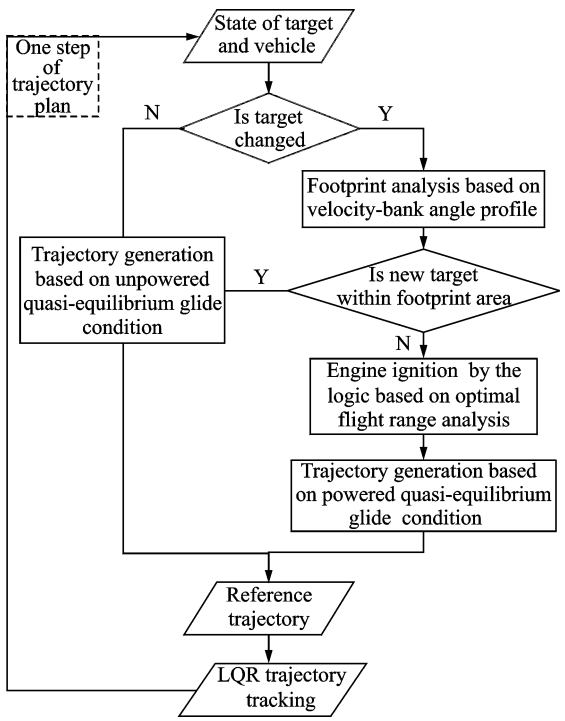


Fig. 1 Adaptive constrained on-board guidance for powered glide vehicle

# 1 Constrained Predictor-Corrector Guidance

## 1.1 Flight condition

The whole trajectory of powered glide vehicle

is composed of four phases(Fig. 2): Boost, inertial, glide, and press. The last three phases are studied here. The 3DOF(Degree of freedom) dimensionless equations of motion for the unpowered vehicle over a spherical rotating earth are described in Ref. [11].

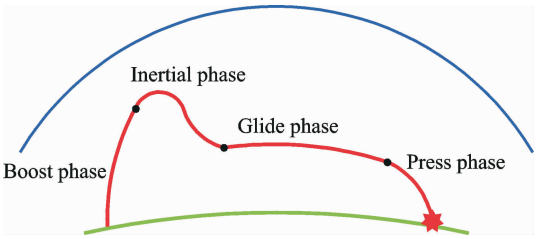


Fig. 2 Four phases of the whole trajectory

Considering the demand of the vehicle′s task, structure, and guidance navigation control (GNC) system, the constraints given in Table 1 should be satisfied during flight.

**Table 1 Flight constraint**

| Constraint | Value |
|---|---|
| Maximum overload | $\leqslant 8$ |
| Range/km | 800—2 500 |
| Terminal velocity/(m·s$^{-1}$) | 450—900 |
| Terminal flightpath angle/(°) | 70±2 |
| Terminal attack angle/(°) | $\leqslant 1$ |
| Maximum attack angle/(°) | $\leqslant 15$ |
| Maximum height/km | $\leqslant 50$ |
| Engine ignition height/km | $\leqslant 45$ |
| Ignition time interval/s | $\geqslant 5$ |

## 1.2 Powered quasi-equilibrium glide condition

The powered trajectory of quasi-equilibrium glide is first designed to satisfy the constraints. Ignoring the rotation of the Earth, the rate of the flight path angle can be derived from the motion equation of longitudinal plane.

$$\dot{\gamma}=\frac{1}{V}\left[(L+P\sin\alpha)\cos\sigma+\left(V^2-\frac{1}{r}\right)\left(\frac{\cos\gamma}{r}\right)\right] \tag{1}$$

where $L$ represents the lift force, which is a function of attack angle $\alpha$; $P$ represents the thrust, which is the main difference from traditional unpowered quasi-equilibrium glide condition. $\gamma$ represents the flight path angle, $V$ the velocity, $\sigma$ the bank angle of velocity, and $r$ the magnitude of position. Since the quasi-equilibrium glide condition required $\dot{\gamma}\approx 0, \gamma\approx 0$, the equation of quasi-equilibrium glide condition is

$$(L+P\sin\alpha)\cos\sigma+\left(V^2-\frac{1}{r}\right)\frac{1}{r}=0 \tag{2}$$

When one of attack angle $\alpha$ and bank angle of velocity $\sigma$ is given, the other angle can be obtained through the iteration of the equation.

## 1.3 Velocity-bank angle profile

The standard atmospheric density model is written in exponential form. Therefore, the path constraints of heating rate, normal acceleration or load factor, and dynamic pressure are as follows

$$h\geqslant h_s\ln\frac{\rho_0 V^{6.5}C_q^2}{Q_{\max}^2} \tag{3}$$

$$h\geqslant h_s\ln\frac{C_y S_{\text{ref}}\rho_0 V^2}{2mg_0 n_{\max}} \tag{4}$$

$$h\geqslant h_s\ln\frac{\rho_0 V^2}{2q_{\max}} \tag{5}$$

In order to determine the flight corridor, the reference attack angle profile must first be given. Referring to the idea of the space shuttle nominal reentry reference attack angle curve design, the attack angle curve is a piecewise linear function of speed.

According to the quasi-equilibrium glide condition and path constraints, velocity-height profile is obtained in Fig. 3. There is a couple of $r_{\min}$ and $r_{\max}$ for every velocity according to the velocity-height profile. Then the upper bound of the bank angle $|\sigma|_{\max}$ is determined by all path constraints, and the lower bound of bank angle $|\sigma|_{\min}=\sigma_{\text{EQ}}$ is obtained by the quasi-equilibrium glide condition.

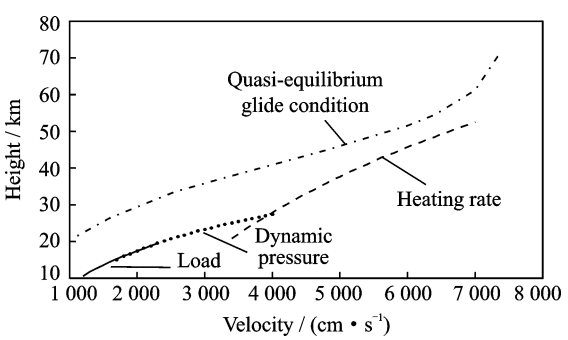


Fig. 3 Velocity-height profile

## 1.4 Bank angle in initial descent

In initial descent, the aerodynamic lift is ineffective in correcting the trajectory in short term, but the bank angle during this period still

has non-trivial effects on the subsequent trajectory. The mechanism based on the quasi-equilibrium glide condition that will be used for path constraint enforcement after the initial descent is not effective in this phase. In the following, we identify the constant upper bound on the magnitude of bank angle $\sigma_{\text{initialmax}}$ during this initial descent phase. This bound will ensure that a bank angle during this initial descent will not violate the heating rate constraint.

From the given initial condition, numerically integrate the equations of motion with a constant bank angle $\sigma_{\text{initial}}$. The integration stops when the following condition is met at some velocity $V_{\text{PT}}$

$$\left| \frac{\mathrm{d}h}{\mathrm{d}V} - \left(\frac{\mathrm{d}h}{\mathrm{d}V}\right)_{\text{QEGC}} \right| < \delta \tag{6}$$

where $\delta > 0$ is a small pre-selected positive value and

$$\frac{\mathrm{d}h}{\mathrm{d}V} = \frac{V\sin\theta}{-\dfrac{D}{m} - g\sin\theta} \tag{7}$$

which is obtained by dividing the equation for $\dot{r}$ with the equation for $\dot{V}$ in the equations of motion. $\left(\dfrac{\mathrm{d}h}{\mathrm{d}V}\right)_{\text{QEGC}}$ is obtained by treating $r$ as a function of $V$ from the equation of quasi-equilibrium glide condition and then take the derivative of $r$ with respect to $V$

$$\left(\frac{\mathrm{d}h}{\mathrm{d}V}\right)_{\text{QEGC}} = \frac{Vh_s\left[2m\cos\theta + C_L\rho S(R_e+h)\cos\upsilon\right]^2}{mg\cos\theta\left[2mh_s\cos\theta + C_L\rho S(R_e+h)^2\cos\upsilon\right]} \tag{8}$$

A simple Newton-Secant method is used to easily find the constant $\sigma_{\text{initial}}$ such that at the point $V_{\text{PT}}$ where Eq. (8) is met, the heating rate constraint is also satisfied. $\sigma_{\text{initial}}$ is designated to be the upper bound $\sigma_{\text{initialmax}}$ found for the bank angle during the initial descent.

### 1.5 Trajectory generation

From the given current condition, longitudinal guidance determines the bank angle magnitude profile $\sigma(V)$ subject to the bound constraints such that the range-to-go $S_{\text{togo}}$ is equal to the required value.

$$S_{\text{togo}} = S_{\text{required}} \tag{9}$$

$$\dot{S}_{\text{togo}} = -V\cos\gamma\cos\Delta\Psi/r \tag{10}$$

where $\Delta\Psi$ represents the azimuth angle offset. Eq. (10) is transferred to the form of velocity-dependent

$$\frac{\mathrm{d}V}{\mathrm{d}S_{\text{togo}}} = \left(\frac{1}{r} - V^2\right)\frac{(C_{\text{D}}/C_{\text{L}})}{V\cos\sigma\cos\Delta\Psi} - P(\sin\alpha + r\cos\alpha)\frac{(C_{\text{D}}/C_{\text{L}})}{V\cos\Delta\Psi} \tag{11}$$

The magnitude of bank angle $\sigma$ is iteratively sought to meet the condition in Eq. (11). The major difference between this method and other algorithms is that the bounds are applied to limit the magnitude of the bank angle along the trajectory in the numerical process. Let $\sigma_{\text{mid}}$ be the constant bank angle magnitude being searched in any iteration. Along the trajectory at any given $V$, the actual bank angle applied in the trajectory integration is given by

$$\sigma = \begin{cases} \sigma_{\text{EQ}}(V) & \sigma(V) < \sigma_{\text{EQ}}(V) \\ \sigma(V) & \sigma_{\text{EQ}}(V) \leqslant \sigma(V) < \sigma_{\max}(V) \\ \sigma_{\max}(V) & \sigma(V) > \sigma_{\max}(V) \end{cases} \tag{12}$$

The profile defined by Eq. (11) enforces all the path constraints, to the extent of the accuracy of QEGC. The sign of bank angle is determined by lateral guidance which is not discussed here. With the magnitude and sign of the bank angle specified, the dynamic equations are numerically integrated from the current condition to target. The predicted range-to-go $S_{\text{togo}}$ is then compared to $S_{\text{required}}$, and the mismatch is used to adjust $\sigma_{\text{mid}}$. The secant method below is found to be effective toward this purpose

$$\sigma_{\text{mid}}^{(i+1)} = \sigma_{\text{mid}}^{(i)} - \frac{\sigma_{\text{mid}}^{(i)} - \sigma_{\text{mid}}^{(i-1)}}{S_{\text{togo}}^{(i)} - S_{\text{togo}}^{(i-1)}}\left(S_{\text{togo}}^{(i)} - S_{\text{required}}\right) \tag{13}$$

Once $\sigma_{\text{mid}}$ is found, $\sigma_0$ and $\sigma_f$ are determined by initial and final states, so will be curve $\sigma(V)$.

## 2 Footprint Analysis Based on Velocity-Bank Angle Profile

Inspired by the acceleration-energy profile, a footprint analysis method based on velocity-bank angle profile is proposed. According to the current flight state and through limiting the bound of the vehicle bank angle, the method can generate a footprint area in which the terminal height and velocity constraints are rapidly satisfied, and

judge whether the desired terminal position is within the area.

### 2.1 Footprint generation

The vehicle attack angle is determined by the velocity-attack angle profile. The upper bound of bank angle $\sigma_{max}$ is limited by the path constraints of heating rate, normal acceleration or load factor and dynamic pressure, and the lower bound of bank angle $\sigma_{min}$ is limited by the quasi-equilibrium glide condition, as shown in Fig. 4. Therefore, the realistic bank angle $\sigma_{real}$ is between $\sigma_{min}$ and $\sigma_{max}$, namely

$$\sigma_{real} = k_1 \sigma_{max} + (1 - k_1)\sigma_{min} \quad k_1 \in (0,1) \quad (14)$$

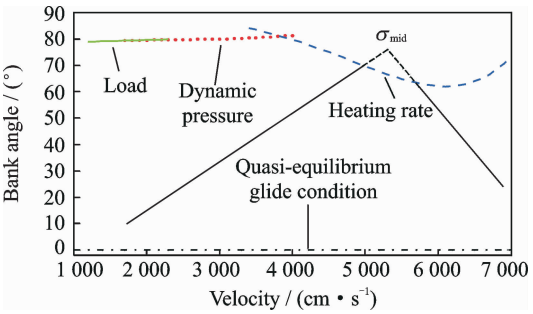


Fig. 4 Velocity-bank angle curve

Therefore, the downrange is the longest when $\sigma_{real} = \sigma_{min}$, the shortest when $\sigma_{real} = \sigma_{max}$, and middle when $\sigma_{min} < \sigma_{real} < \sigma_{max}$. The crossrange varies with the azimuth angle. Footprint area diagram is given in Fig. 5, where the footprint boundary is the line connecting eight boundary points (the dot) and the target (the star) is within the footprint.

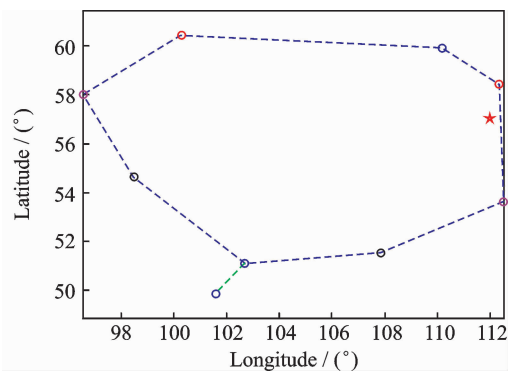


Fig. 5 Footprint area diagram

### 2.2 Footprint judgment

The method of judging whether the target is within the footprint here is called "the sum of the interior angles". The principle of this method is that the sum of the interior angles will be 360° when the target is within the footprint; otherwise, the sum will less than 360°.

## 3 Ignition Time Analysis with Optimal Flight Range

The ignition time of a double-pulse rocket engine, which has a great influence on the flight range of the glide vehicle, is a necessary parameter for the powered on-board trajectory generation. The hp-adaptive Gauss pseudospectral method, which can effectively solve problems with discontinuous dynamics, is employed to give an optimization analysis of variation between flight range and ignition time of the pulse engine. The double-pulse rocket engine performance is given in Table 2.

**Table 2 Double-pulse rocket engine performance**

| Number of pulse | Work time/s | Average thrust/N | Rate of fuel consumption/(kg • s) |
|---|---|---|---|
| First | 27.4 | 50 549.4 | 18.61 |
| Second | 16.6 | 53 000.2 | 18.86 |

On the condition of ignition once, the ignition time varies from 0 to 290 s after boost. The variation of flight range along with ignition time is shown in Fig. 6. The result shows that the earlier the engine ignites, the further the vehicle flies.

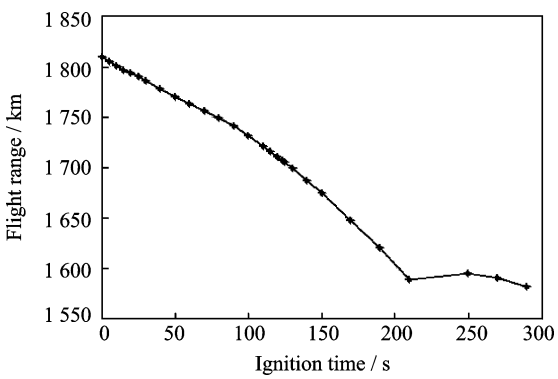


Fig. 6 Flight range along with ignition time for ignition once

On the condition of ignition twice, the time of the first ignition is fixed at 0 s, and the time of the second ignition varies from 0 to 290 s after the

first ignition. The variation of flight range along with ignition time is shown in Fig. 7.

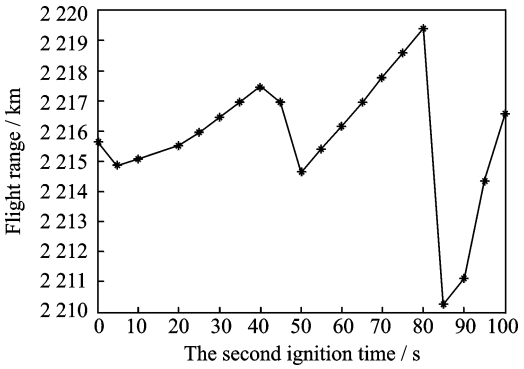


Fig. 7 Flight range along with ignition time for ignition twice

The result shows that the variation of flight range along with the second ignition time is not monotonous. The constraint of the maximum flight height and height of engine ignition is one of the reasons. Meanwhile, the difference between flight ranges of different ignition time spans is not big, because, after the first ignition, the flight height of the vehicle causes the aerodynamic force relatively small. Therefore, the increased energy by the second ignition is similar. The best time of the second ignition is given by optimization.

To obtain the effect of the flight range increased by double-pulse rocket engine, the hp-adaptive Gauss pseudospectral method is employed to give an optimization analysis of variation between flight range and ignition times of the pulse engine. The optimization results are shown in Table 3.

**Table 3 Optimization results of ignition times and range**

| Ignition time | Flight range/km | Flight time/s |
|---|---|---|
| Unpowered reference | 1 084.51 | 662.01 |
| Unpowered optimization | 1 082.84 | 652.65 |
| Ignition once optimization | 1 850.01 | 1 003.95 |
| Ignition twice optimization | 2 413.87 | 1 167.45 |

The results show that the optimal flight range of unpower is more than 1 000 km, the optimal flight range of ignition once is more than 1 400 km, and the optimal flight range of ignition twice is more than 2 400 km. Obviously, the optimal flight range of unpower is little less than that of the reference trajectory because the reference trajectory dose not satisfy all the constraints. This means that searching solution satisfying all the constraints is one of the important functions of trajectory optimization.

## 4 Simulation

To show the accuracy, efficiency, and reliability of the proposed method, two groups of simulation scenarios, target position variation and ignition time variation, are presented. The simulation program is written in $C^{++}$ language, and operates on the computer with 2.0 GHz CPU clock speed.

All the cases use the same vehicle parameters, mass property, propulsion system modeling, and aerodynamic modeling of some vehicle with a double-pulse rocket engine. The feasible reference trajectory and reference profile of the angle of attack and bank angle are obtained by a powered on-board trajectory generation method. The LQR method is used to track the generated trajectory to precisely reach the target in a variety of the desired terminal position. The values of simulation parameters are provided in Table 4.

**Table 4 Simulation parameters**

| Parameter | Name | Value |
|---|---|---|
| Initial state | Mass/kg | 2 132.4 |
| | Velocity/(m·s$^{-1}$) | 2 922 |
| | Flight path angle/(°) | 0.292 |
| | Azimuth angle/(°) | 11 |
| | Altitude/km | 50 |
| | Longitude/(°) | 100.805 |
| | Latitude/(°) | 47.385 |
| Old target | Altitude/km | 20 |
| | Longitude/(°) | 107 |
| | Latitude/(°) | 59 |
| New target | Altitude/km | 20 |
| | Longitude/(°) | Variation |
| | Latitude/(°) | Variation |
| Constraint | Overload | 8 |
| | Dynamic pressure/kPa | 300 |
| Ignition time | Variation | |
| Attack angle | Profile of the biggest lift-drag ratio | |

### 4.1 Target position variation

Taking ignition time as 55 s after boost, the new footprint area after ignition is shown in Fig. 8.

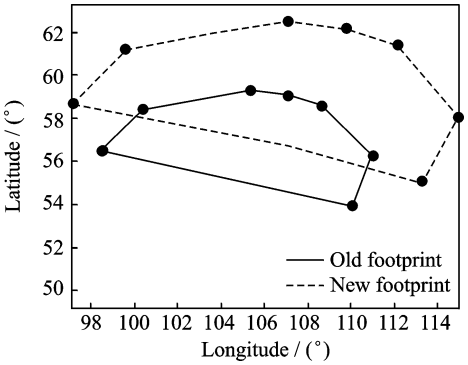


Fig. 8 Old and new footprints

Taking the seven end points and one inner point as new targets, simulation of on-board trajectory generation and guidance is conducted. The position of news targets are shown in Table 5, and simulation results are as follows. Altitude histories and footprint area are shown in Figs. 9, 10, respectively for the target No. 8.

**Table 5 Position of new targets**

| No. | Longitude/(°) | Latitude/(°) |
|---|---|---|
| 1 | 109.8 | 62.2 |
| 2 | 107 | 62.5 |
| 3 | 112.13 | 61.45 |
| 4 | 99.6 | 61.2 |
| 5 | 114.9 | 58.03 |
| 6 | 97 | 58 |
| 7 | 113.26 | 55 |
| 8 | 110 | 60 |

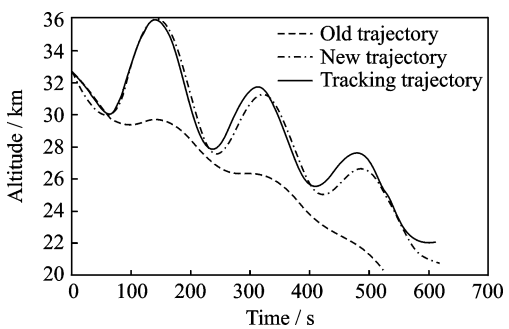


Fig. 9 Altitude histories for trajectory generation and tracking of target No. 8

The simulation results are summarized in Tables 6, 7. The results show that the adaptive constrained on-board trajectory generation method based on the footprint analysis can plan a new trajectory within 0.66 s for different targets. And the final errors of the LQR guidance is relatively small: Average longitude deviation is 0.053 7°, and average latitude deviation is 0.123 7°.

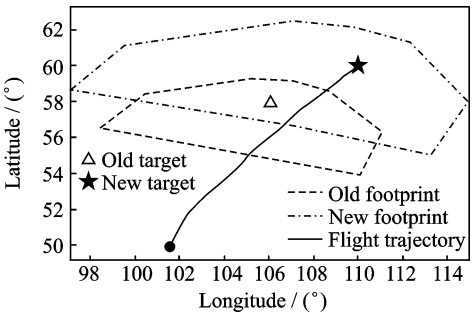


Fig. 10 Footprint area diagram for trajectory generation and tracking of target No. 8

**Table 6 Results of simulation when target position varying**

| No. | (Target Lon/Lat)/(°) | (Generation Lon/Lat)/(°) | (Guidance Lon/Lat)/(°) |
|---|---|---|---|
| 1 | 110.5/63.0 | 109.8/62.2 | 109.7/62.2 |
| 2 | 107.8/63.3 | 107/62.53 | 107.02/62.47 |
| 3 | 113.133/62.3 | 112.13/61.45 | 112.10/61.54 |
| 4 | 99.9/62.2 | 99.6/61.2 | 99.72/61.29 |
| 5 | 116.3/58.6 | 114.993/58.03 | 115.00/58.00 |
| 6 | 96.4/59.5 | 97/58 | 96.962/58.64 |
| 7 | 114.66/55.50 | 113.261/55.004 | 113.28/55.047 |
| 8 | 111.1/60.8 | 110/60 | 110.09/60.038 |

**Table 7 Time of simulation when target position varying**

| No. | Old trajectory/s | New footprint/s | New trajectory/s |
|---|---|---|---|
| 1 | 0.531 | 0.795 | 0.624 |
| 2 | 0.422 | 0.669 | 0.565 |
| 3 | 0.501 | 0.605 | 0.542 |
| 4 | 0.499 | 0.613 | 0.603 |
| 5 | 0.562 | 0.588 | 0.657 |
| 6 | 0.497 | 0.516 | 0.556 |
| 7 | 0.405 | 0.366 | 0.435 |
| 8 | 0.577 | 0.573 | 0.607 |

## 4.2 Ignition time variation

Taking new target longitude/latitude as 100°/60°, ignition time varies from 10 s to 300 s after boost, and the simulation results of on-board trajectory generation and guidance are as follows. Altitude histories, footprint area and bank angle history are shown in Figs. 11—13, respectively when igniting at 60 s.

The simulation results are summarized in Tables 8, 9. The results show that the adaptive constrained on-board trajectory generation method based on the footprint analysis can plan a new trajectory within 0.7 s for different ignition

times. And the final errors of LQR guidance is acceptable: Average terminal velocity deviation is 5.914 m/s, and average terminal height deviation is 1 136.1 m.

**Table 8 Results of simulation when ignition time varying**

| No. | Ignition time/s | Terminal velocity deviation/(m·s$^{-1}$) | Terminal height deviation/m |
|---|---|---|---|
| 1 | 10 | 5.788 | 1 069.2 |
| 2 | 20 | 2.035 | 1 271.2 |
| 3 | 30 | 3.914 | 1 299.3 |
| 4 | 40 | 4.35 | 1 313.1 |
| 5 | 60 | 9.051 | 1 201.5 |
| 6 | 80 | 8.338 | 1 221.8 |
| 7 | 100 | 6.455 | 1 133.2 |
| 8 | 120 | 1.99 | 1 037.2 |
| 9 | 150 | 4.03 | 996.01 |
| 10 | 180 | 8.46 | 963.3 |
| 11 | 210 | 9.17 | 1 016.5 |
| 12 | 240 | 3.22 | 1 009.33 |
| 13 | 270 | 1.235 | 1 187.1 |
| 14 | 300 | 14.76 | 1 186.5 |

**Table 9 Time of simulation when ignition time varying**

| No. | Old trajectory/s | New footprint/s | New trajectory/s |
|---|---|---|---|
| 1 | 0.422 | 0.669 | 0.587 |
| 2 | 0.514 | 0.756 | 0.618 |
| 3 | 0.469 | 0.675 | 0.569 |
| 4 | 0.506 | 0.635 | 0.549 |
| 5 | 0.611 | 0.712 | 0.563 |
| 6 | 0.493 | 0.599 | 0.619 |
| 7 | 0.557 | 0.625 | 0.649 |
| 8 | 0.567 | 0.645 | 0.529 |
| 9 | 0.438 | 0.526 | 0.658 |
| 10 | 0.550 | 0.615 | 0.599 |
| 11 | 0.613 | 0.518 | 0.612 |
| 12 | 0.649 | 0.638 | 0.573 |
| 13 | 0.589 | 0.705 | 0.622 |
| 14 | 0.532 | 0.672 | 0.511 |

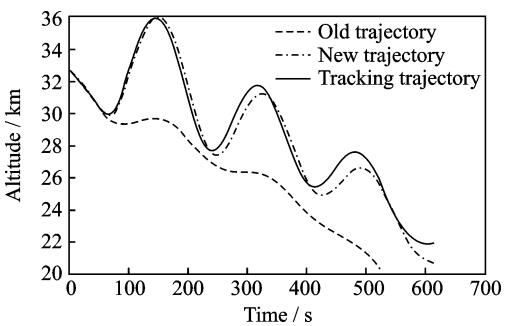


Fig. 11 Altitude histories for trajectory generation and tracking when igniting time of 60 s

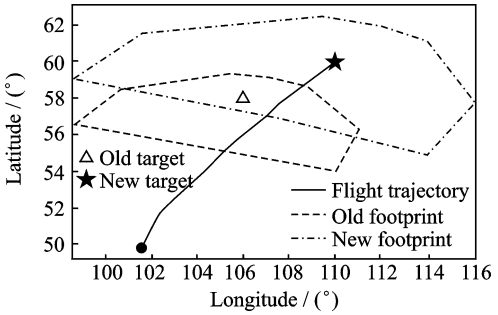


Fig. 12 Footprint area diagram for trajectory generation and tracking with igniting time of 60 s

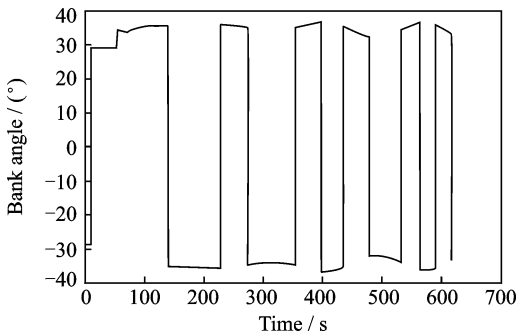


Fig. 13 Bank angle history for trajectory generation and tracking with igniting time of 60 s

## 5 Conclusions

Simulation under the various conditions are implemented to indicate the applicability and effectiveness of the adaptive constrained on-board guidance technology consisted of powered on-board trajectory generation, footprint calculation, ignition time determination, and LQR trajectory tracking. The presented simulation results show that a double-pulse rocket engine can increase 120% of flight range compared with the unpowered glide vehicle, and the proposed approach can generate a feasible trajectory in 0.7 s with small deviation for different target positions and ignition times.

The footprint area of the glide vehicle is expanded by using the multi-pulse rocket engine, which makes it possible for the glide vehicle to reach more desired terminal positions combined with the proposed footprint analysis method and powered on-board trajectory generation and track method. Future work will focus attention on exploring the other contributions of multi-pulse rocket engine and the on-board trajectory genera-

tion method, such as penetration with bigger velocity and on-line reconfigurable control and guidance, etc.

**Acknowledgements**

This work was supported by the National Natural Science Foundation of China (No. 61403100) and Fundamental Research Funds for the Central Universities (HIT. NSRIF. 2015037).

**References:**

[1] CRAIG P. Preliminary pulse motor optimization for a surface-to-air missile[C]// AIAA Guidance, Navigation and Control Conference. Monterey, CA: AIAA, 1993:355-362.

[2] CRAIG P. Energy management for multiple-pulse missiles[J]. Journal of Spacecraft and Rockets, 1990, 27(6): 623-629.

[3] JOHN M H, ROBERT E J. Test results for entry guidance methods for space vehicles[J]. Journal of Guidance, Control, and Dynamics, 2004, 27(6): 960-966.

[4] LU P. Entry Guidance: A unified method[J]. Journal of Guidance, Control, and Dynamics, 2014, 37(3): 713-728.

[5] BRAUN R D, POWELL R W. Predictor-corrector guidance algorithm for use in high-energy aerobraking system studies[J]. Journal of Guidance, Control, and Dynamics, 1992, 15(3): 672-678.

[6] ZIMMERMAN C, DUKEMAN G, HANSON J. Automated method to compute orbital reentry trajectories with heating constraints[J]. Journal of Guidance, Control, and Dynamics, 2003, 26(4): 523-529.

[7] LU P. Predictor-corrector entry guidance for low lifting vehicles[J]. Journal of Guidance, Control, and Dynamics, 2008, 31(4): 1067-1075.

[8] LU P. Asymptotic analysis of quasi-equilibrium glide in lifting entry flight[J]. Journal of Guidance, Control, and Dynamics, 2006, 29(3): 662-670.

[9] SHEN Z, LU P. Onboard generation of three-dimensional constrained entry trajectories[J]. Journal of Guidance, Control, and Dynamics, 2003, 26(1): 111-121.

[10] AMITABH S, LEAVITT J A, MEASE K D. Landing footprint computation for entry vehicles[C]// Providence, Rhode Island: AIAA Guidance, Navigation, and Control Conference and Exhibit. Providence, Rhode Island: AIAA, 2004:1-14.

[11] ZHANG Rui, LI Zhaoying, SHI Linan. A general footprint generation approach for lifting re-entery vehicle[C]// 28th International Congress of the Aeronautical Sciences. Brisbane Australia: ICAS, 2012:1-7.

[12] HANSON J, JONES R. Advanced guidance and control methods for reusable launch vehicles[C]// Guidance, Navigation and Control Conference and Exhibit. Monterey, California: AIAA, 2002:1-14.

[13] LU P, XUE Songbai. Rapid generation of accurate entry landing footprints[J]. Journal of Guidance, Control, and Dynamics, 2010, 33(3):756-767.

[14] LI Y, CUI N G. Optimal attack trajectory for hypersonic boost-glide missile in maximum reachable domain[C]// Proceedings of the 2009 IEEE International Conference on Mechatronics and Automation. Changchun, China: IEEE, 2009:4012-4017.

[15] RICHARDS N D, SHARMAN M, WARD D G. A hybrid star automation approach to online path planning with obstacle avoidance[C]// AIAA 1st Intelligent Systems Technical Conference. Chicago: AIAA, 2004: 1-17.

[16] HUNTINGTON G T, BENSON D, RAO A V. A comparison of accuracy and computational efficiency of three pseudospectral methods[C]// AIAA Guidance, Navigation and Control Conference and Exhibit. Hilton Head, South Carolina: AIAA, 2007:1-43.

[17] SUN Yong. Trajectory optimization and guidance of hypersonic vehicle based on improved Gauss pseudospectral method[D]. Harbin: Harbin Institute of Technology, 2012. (in Chinese)

[18] VINH N X. Optimal trajectories in atmospheric flight[M]. New York: Elsevier, 1981.

Mr. **Huang Rong** is a Ph. D. candidate in Aircraft Design from School of Astronautics, Harbin Institute of Technology. His main research interests are overall design of aircraft, trajectory optimization, guidance, and control.

Dr. **Wei Changzhu** is an associate professor in School of Astronautics, Harbin Institute of Technology(HIT). He received his Ph. D. degree in HIT. His research interests are aircraft dynamics, formation flight cooperative guidance and control.

Dr. **Liu Yanbin** is an associate professor in College of Astronautics, Nanjing University of Aeronautics and Astronautics (NUAA). He received his Ph. D. degree in NUAA. His research interests are flight control.

Prof. **Lu Yuping** is working in College of Astronautics, Nanjing University of Aeronautics and Astronautics (NUAA). His research interests are spacecraft control, flight control.

(Executive Editor: Xu Chengting)